JOURNAL OF MATERIALS SCIENCE **36** (2001) 1513–1522

Strengthening and toughening mechanisms in microfiber reinforced cementitious composites

CK. YI, C. P. OSTERTAG
Civil Engineering Department, University of California, Berkeley, CA.94720, USA
E-mail: ostertag@ce.berkeley.edu

Materials with quasi-brittle stress strain curves exhibit desirable properties such as enhanced durability, flaw tolerance and toughness. This study reveals that steel microfiber reinforced cement based composites exhibit such quasi-brittle behavior. Mechanical properties of steel microfiber reinforced cement based composites are obtained through flexure and splitting tension tests. The cracking process and crack fiber interactions that lead to the quasi-brittle behavior in these composites were investigated. The strength and toughness enhancement is associated with crack wake mechanisms. Aggregate bridging and pullout and secondary crack formations associated with microfiber bridging sites are predominant during the strain hardening regime. Multiple secondary microcracks perpendicular to the fiber/matrix interface is the dominant failure mode beyond peak load in the strain softening regime.

1. Introduction

The stress-strain curve of a quasi-brittle material generally consists of three regions corresponding to the different mechanisms that control the behavior of the composite. The first region corresponds to the linear elastic response of the composite. The point at which the stress-strain curve becomes nonlinear (bend over point (BOP)) exceeds the cracking stress of the unreinforced matrix material. Hence, higher stresses are required for matrix crack initiation. The second region is associated with strain hardening where the strength increases beyond the BOP up to a maximum. This maximum corresponds to the ultimate strength of the composite. The third region, where the composite gradually loses its load carrying capacity, is associated with the strain softening regime. Materials with this type of quasi-brittle behavior exhibit desirable properties such as enhanced durability, flaw tolerance and toughness.

In conventional fiber reinforced cement based composites the fibers that are commonly used only contribute to the strain softening regime, and the improvement in tensile strength is negligible [1, 2]. The matrix cracking stress is the ultimate strength of the composite. The typical fibers used in these composites are 500 μm in diameter and 25–50 mm in length. The effect of these fibers comes into play after macrocrack initiation and continued opening of the crack is restrained by the fibers leading to the post peak softening behavior. The maximum amount of fibers that can be incorporated is 2 vol% due to their detrimental effect on workability of the concrete mix. In order to enhance the tensile strength, small cracks need to be arrested and their coalescence into a dominant macrocrack delayed to higher stress levels. Small cracks are present in the cement based materials even before load application due to drying shrinkage and/or thermal shrinkage. Macrofibers, due to their large dimensions are only able to bridge and interact with macrocracks. Furthermore, due to the small number of fibers per square inch at 2 vol% these fibers are spaced too far apart to arrest and interact with small cracks. Cement based composites reinforced with microfibers (10–20 μm in diameter and 3–10 mm in length) on the other hand, do exhibit strength enhancement [3, 4]. It is generally believed that microfibers due to their small dimensions and hence increased numerical fiber density are more likely to stabilize and bridge microcracks and other inherent flaws in the material.

The cracking processes in microfiber reinforced cement based composites are not well understood. Investigations that concentrate on the fracture mechanisms in these composites are limited [5]. While most experimental [6–8] and analytical [9–12] research has focused on cracking mechanisms and strength enhancement due to aligned, continuous fibers, little research has focused on short, randomly distributed microfibers. However, a fundamental understanding of these mechanisms is essential in order to tailor and optimize the properties of these composites.

This study was aimed at obtaining information on the strengthening and toughening mechanisms in steel microfiber reinforced composites through *in-situ* crack propagation measurements during load application. Mechanical properties were obtained through flexure and splitting tension tests.

2. Experimental procedure

2.1. Material and mortar mix

The properties of the steel microfibers are given in Table I. Fig. 1a and b, reveal the rectangular

TABLE I Properties of the steel microfibers

Fiber Type	Cross Section	Length (mm)	Elastic Modulus (MPa)	Tensile Strength (MPa)
Steel	(20–40) μm × (100–140) μm	3–5	200,000	410

TABLE II Mix Proportions for the control, C, and the steel microfiber reinforced composites, SFR, at various fiber volume fractions. (All proportions given by weight, except the fiber content)

	W/(C + SF)	SF/C	S/(SF + C)	SP/(SF + C)	Vf(%)
C	0.36	0.23	1.45	0.012	0
SFR 2	0.36	0.23	1.39	0.014	2
SFR 4	0.36	0.23	1.32	0.020	4
SFR 6	0.36	0.23	1.26	0.030	6

cross-sections and surface characteristics of the microfibers. Each fiber exhibits one rough and one slightly smoother surface caused by the fabrication process. The mix design for microfiber reinforced mortar composites used to fabricate cylindrical, beam and compact tension specimens is given in Table II. Mortar specimens without fibers were fabricated as well to serve as control specimens. Lonestar Elliot sand with fineness modulus of 3.09 was used. In addition, silica fume was added. Silica fume acts as a filler material due to its

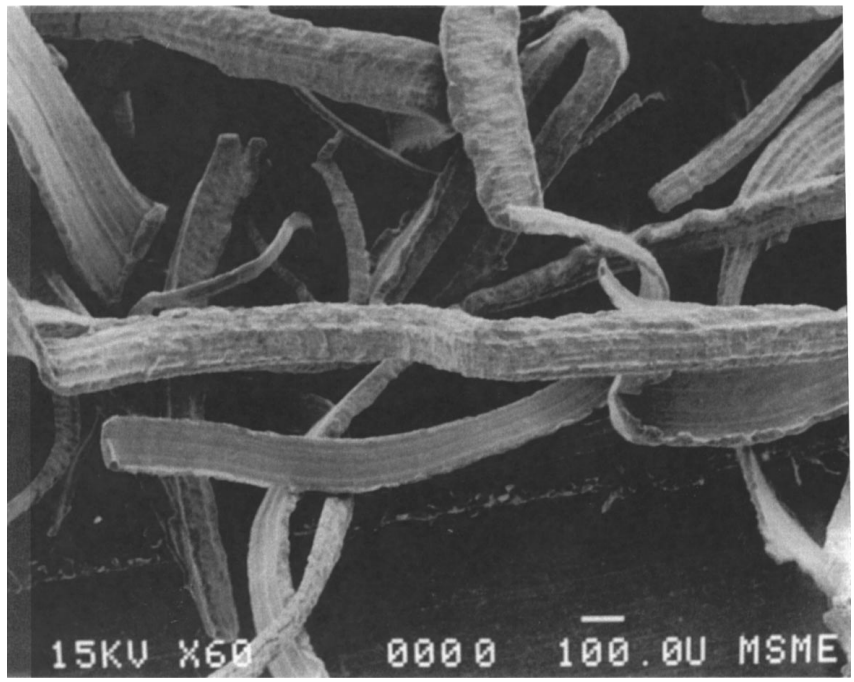

(a)

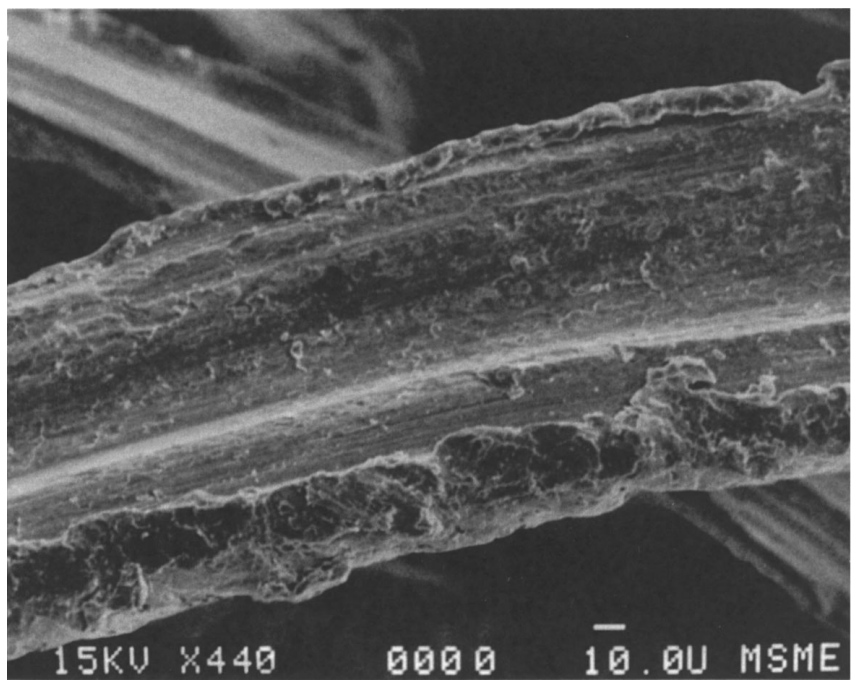

(b)

Figure 1 The rectangular cross-sections and surface characteristics of the steel microfibers; (a) and (b) are SEM micrographs taken at different magnifications.

small particle size and reacts with CH, thereby limiting the amount of the weak CH crystals at the fiber/matrix and aggregate/matrix interface. Consequently a much denser and stronger interfacial zone with improved mechanical properties is expected. Steel microfibers of 2 vol%, 4 vol% and 6 vol% were incorporated into the mortar mix. The amount of superplasticizer increased with volume fraction of fibers to achieve similar workability throughout the different mixes. The formwork of the various test specimens was removed after 24 hours and the specimens were cured in a fog room at 100% relative humidity and 23°C.

2.2. Specimen preparation and testing procedure

2.2.1. Splitting tension and flexure specimens

For the splitting tension tests, 76 mm × 152 mm cylindrical specimens were cast with 0%, 2%, 4% and 6 vol% of steel microfibers and cured for 7 days in a fog room

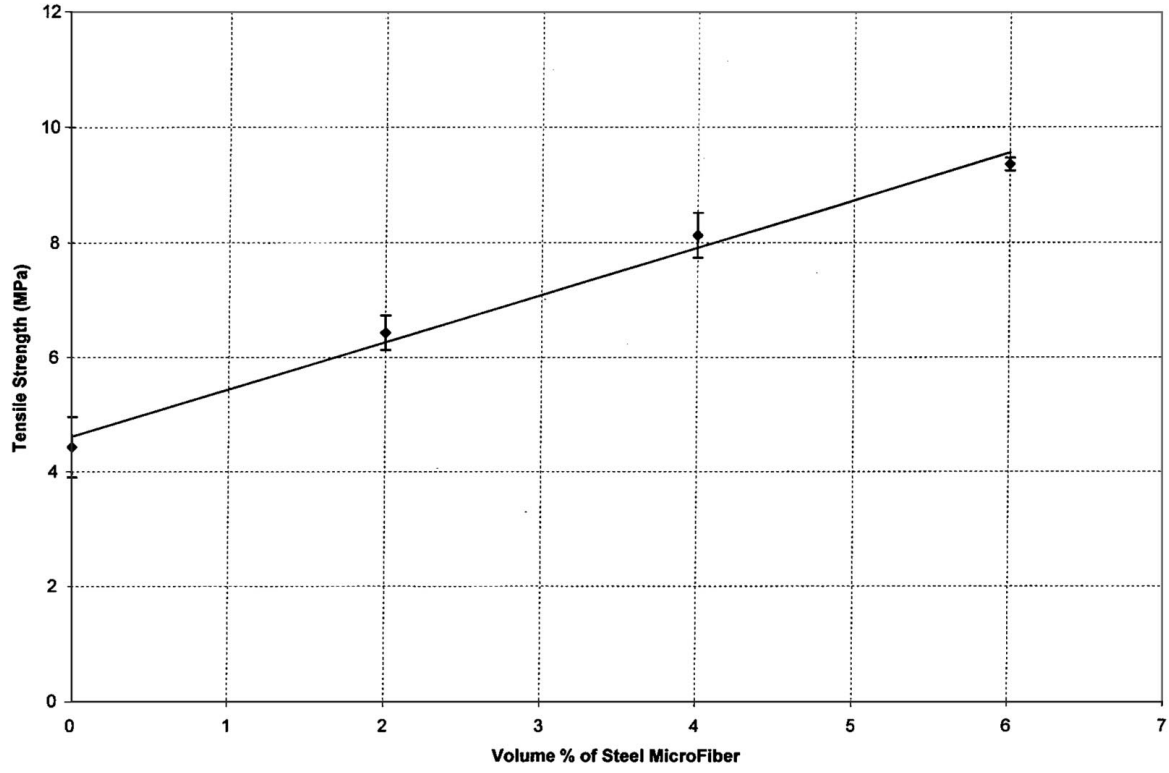

Figure 2 Results of splitting tension test on strength enhancement of mortar composites reinforced with 0, 2, 4, and 6 vol% of steel microfibers after 7 day curing time.

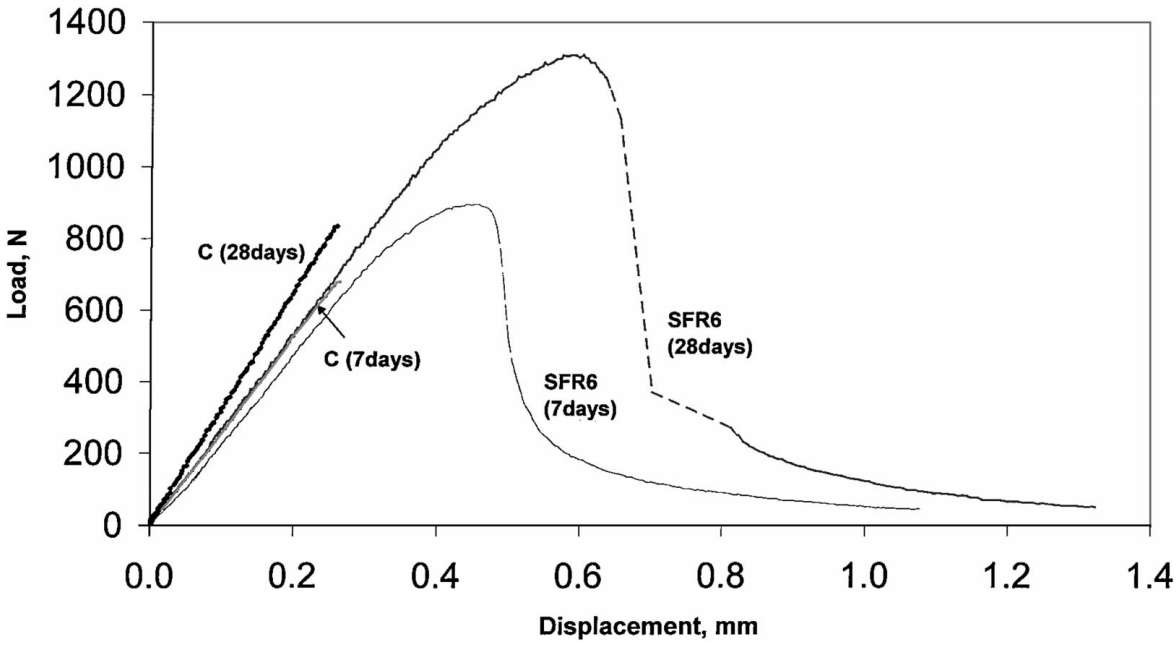

Figure 3 Flexure test results for control mortar specimens and 6 vol% steel microfiber reinforced mortar composites after 7 and 28 days curing time.

TABLE III Properties of the mortar control specimens and 6 vol% steel microfiber reinforced composites after 7 days and 28 days of curing time

	Avg. Max Load (N)		Avg. Load at BOP (N)	
Matrix	7 Day Testing	28 Day Testing	7 Day Testing	28 Day Testing
C	672	836	672	836
SFR6	916	1210	734	947

prior to testing. Three specimens were tested at each fiber volume fraction. The splitting tension test was performed according to ASTM C496.

The flexure tests were performed on 25 mm × 25 mm × 280 mm inch prismatic beams reinforced with 6 vol% of microfibers. The specimens for the flexure tests were first cast in a brass mold of 25 mm × 180 mm × 280 mm size to minimize the wall effect as well as to ensure random orientation of the microfibers. The specimens were cured for 7 days and 28 days, respectively, and six flexure specimens were cut from each slab before testing. Four point bending with loading at the third points was performed on a 50 kip capacity MTS machine. The specimens were loaded under displacement control at a cross arm speed of 0.03 mm/sec. Displacement at mid-span was monitored by an external LVDT in contact with the bottom of the specimen. The loading was terminated when the maximum cross arm displacement of 2.5 mm was reached unless failure preceded the maximum displacement.

2.2.2. Compact tension specimens

Compact tension specimens were fabricated according to the ASTM E 399 specifications. Mortar specimens were cast using 50 mm × 50 mm × 50 mm steel molds. To avoid machining the loading holes for the compact tension specimens, two plexiglas rods were pre-positioned inside the steel molds. For the compact tension specimens, the sand was sieved through a US No. 16 sieve (opening size of 1180 μm) in order to separate the coarse from the finer sand grains. Only the smaller grains were used in the mix to enhance homogeneous distribution of the microfibers and to ensure that the sand grains are much smaller than the thickness of the specimen. The mortar mix was placed in the formwork and vibrated on a vibrating table for about 10 seconds. After 25 days of curing, the cubes were cut into compact tension specimens with a width, W, of 40 mm and a thickness of 8 mm. A constant notch length of 14 mm was used for all specimens. The notch was cut using saw blades of different thickness; 75% of the desired notch length was cut using a saw blade of 2.5 mm thickness and the rest of the notch was cut with a thinner saw of 0.3 mm. The specimens were surface ground to ensure uniform thickness and successively polished with 38 μm SiC powder, 12 μm, 9 μm and 3 μm Al_2O_3 powder to facilitate crack identification under the microscope. Polished specimens were wrapped in plastic and returned to the fog room for three more days to complete the 28 day curing.

The compact tension specimens were loaded under displacement control using a custom designed loading device based on the design by Rodel *et al.* [13] and Frei and Grathwohl [14]. The loading device was staged under an optical microscope. The microscope is equipped with a video camera connected to a TV screen and video recorder. The specimens are loaded by a piezoelectric translator which after being activated by a high voltage amplifier delivers an opening force to the

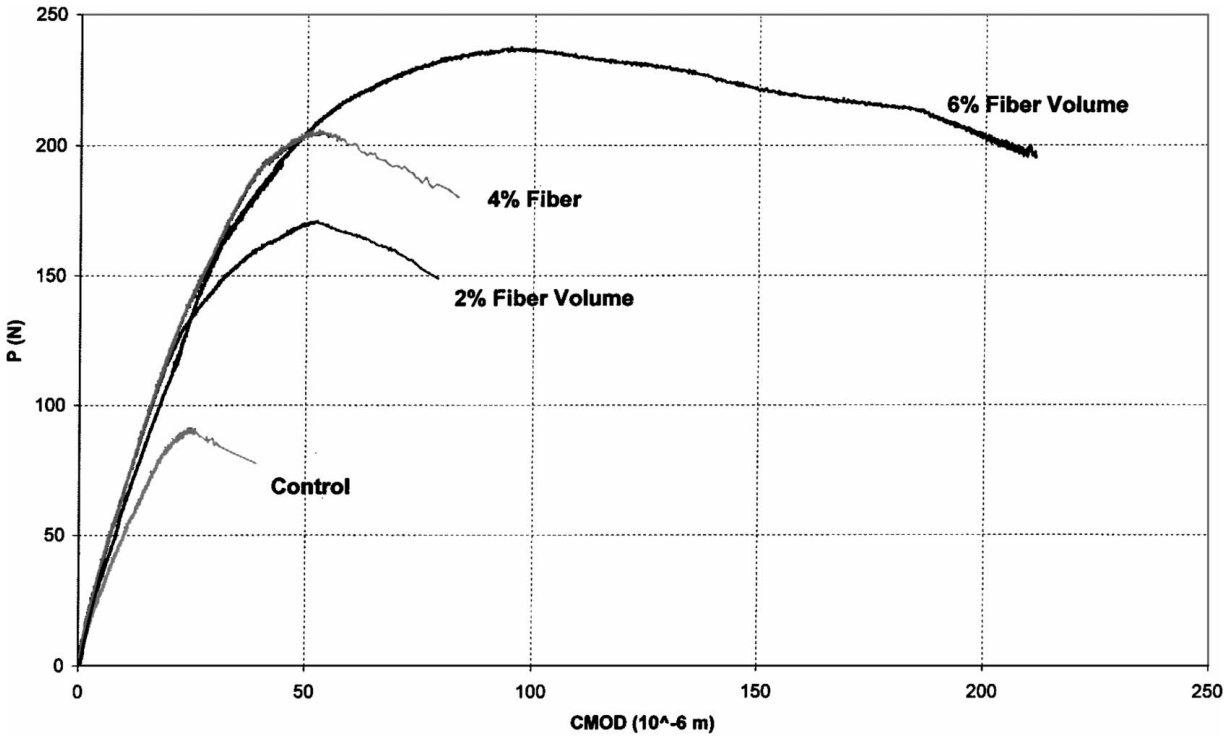

Figure 4 Load versus crack mouth opening displacement (CMOD) curves of compact tension specimens with various steel microfiber volume fractions.

specimen. The input voltage was computer controlled. A load cell is placed in one of the loading arms and monitors the applied load up to 3000 N.

The specimens were precracked using the loading device by slowly loading the specimens until a through thickness crack was obtained. Crack propagation measurements were performed in a controlled room-air environment (22°C, 50% relative humidity) and recorded on video. An MTS clip gage was mounted on the specimen to monitor the crack mouth opening displacement (CMOD). Three specimens were tested for 0, 2, 4 and 6 vol % of microfibers, respectively. All specimens were loaded continuously up to failure. A slow displacement rate of 0.001 mm/sec was chosen for all specimens to be able to observe the cracking process while loading.

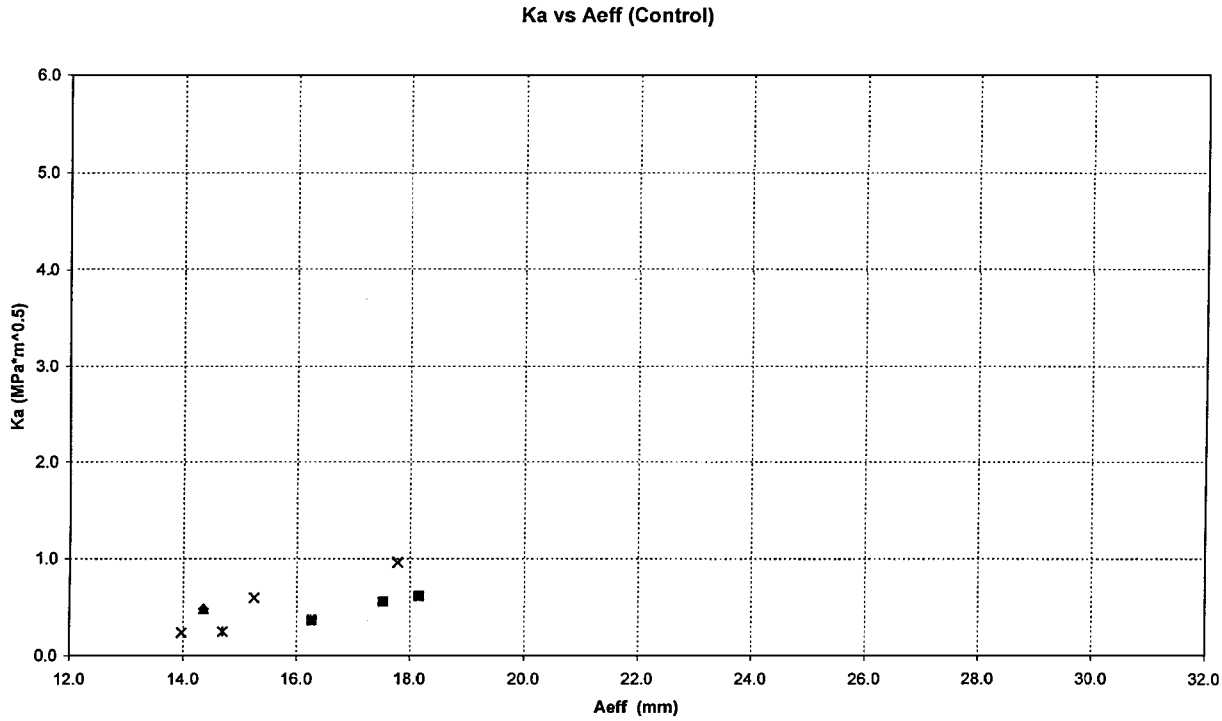

(a)

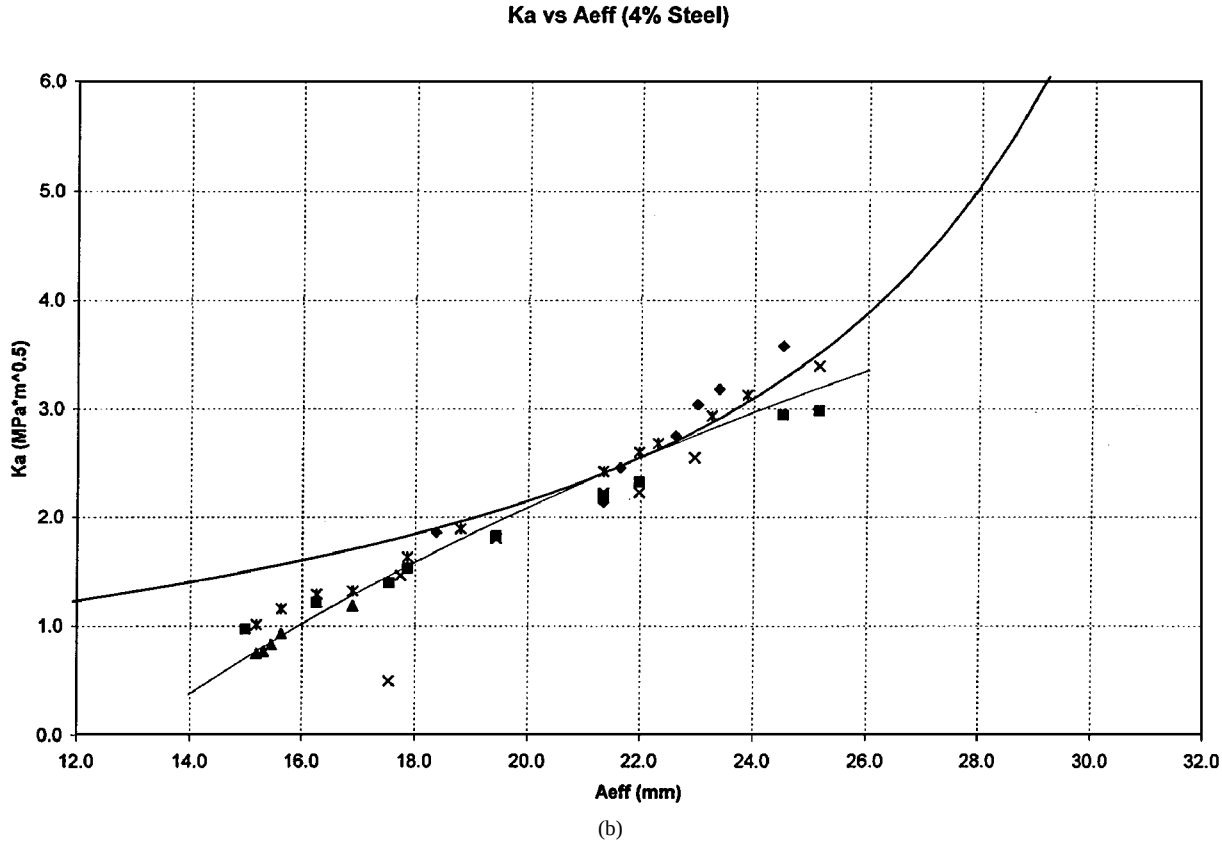

(b)

Figure 5 Crack growth resistance curves for the control mortar specimens (a) and for 4 vol% of steel microfibers (b). The symbols in the graphs represent the experimental data points for different test specimens. Aeff was measured experimentally. A best fit curve (solid curve) through the experimental data points and the K-curve which satisfies the $\partial K/\partial a = \partial Ka/\partial a$ condition is also plotted in b).

3. Results and discussion

3.1. BOP, ultimate strength and toughness enhancement due to microfiber

3.1.1. Splitting tension tests

The ultimate strength of microfiber reinforced mortar composites in the splitting tension tests increases linearly with increasing fiber volume fraction as shown in Fig. 2. This strength enhancement is also accompanied by a decrease in the standard deviation from 11% for the control specimen to 1.2% for the 6 vol% of microfibers. This reduction in standard deviation indicates a lower sensitivity to the flaw size distribution with increasing fiber volume fractions.

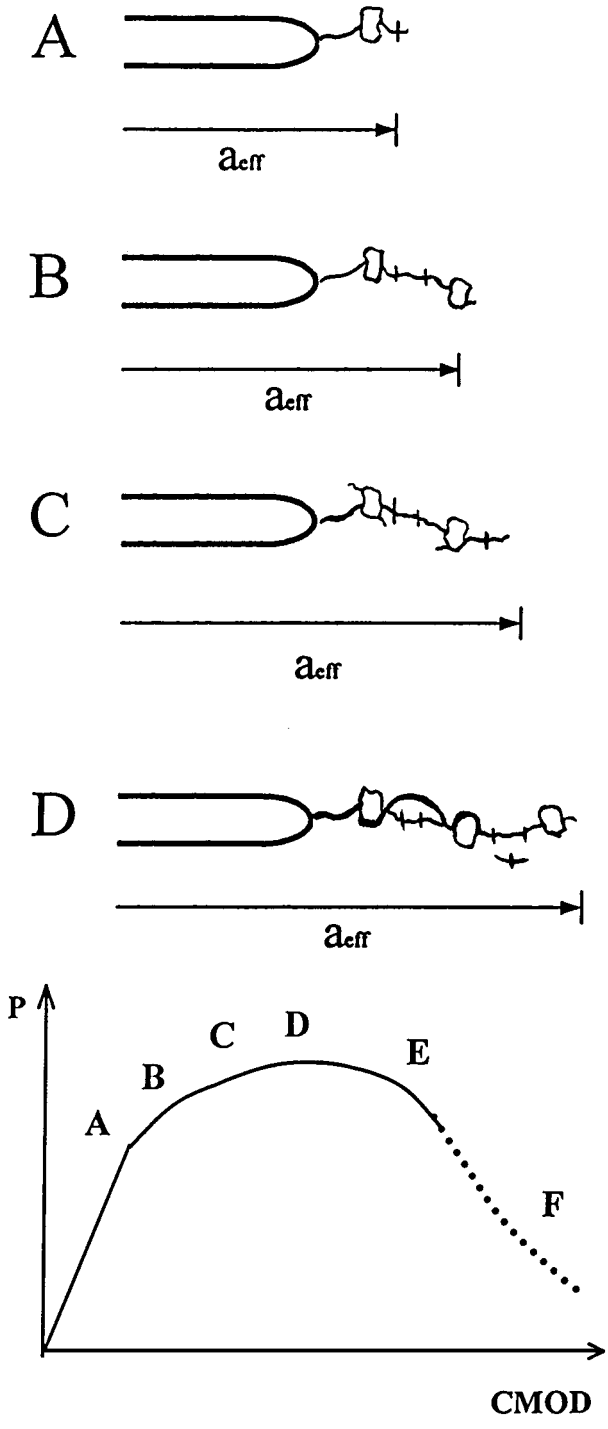

Figure 6 Schematic of the cracking process in microfiber reinforced composites at load levels A–D of the ascending branch in the load-crack mouth opening displacement curve. Crack extension occurs at load level A. The descending branch after point E is indicated by broken lines because a continuous strain softening curve could not be obtained experimentally. The fiber reinforced specimens at position F remained intact, carrying on average a residual load of 70 N.

3.1.2. Flexure tests

The beam tests with 6 vol% of microfibers reveal an increase in the matrix cracking strength (BOP) and an increase in ultimate strength (Fig. 3). The tensile properties of the mortar control specimens and the 6 vol% fiber reinforced composites cured for 7 days and 28 days are shown in Table III. In the control specimens the bend over point coincides with the ultimate strength. Although the strength of the control specimen increases with aging the relative improvement is small compared to the steel microfiber reinforced composites. The increase in ultimate strength of the composites compared to the control specimens is more pronounced after 28 days. The displacement at maximum load is 1.7 and 2.5 times greater than that of the control beams at 7 days and 28 days, respectively. Hence the strain capacity of the mortar is enhanced considerably by the incorporation of the steel microfibers. The high extensibility of our composites is associated with energy absorbing mechanisms associated with aggregate and fiber bridging sites during the strain hardening regime as will be discussed in Section 3.3.

3.1.3. Compact tension tests

Load versus crack mouth opening displacement (CMOD) of compact tension specimens with various fiber volume fractions is shown in Fig. 4. Beyond the peak load, a continuous strain softening curve could not be obtained. The data acquisition system was programmed to collect data at one second intervals. The data points are hence spaced too far apart and omitted in the graph. The ultimate strength and the strain capacity at ultimate strength increased with increasing fiber volume fractions.

3.2. Crack growth resistance behavior

The externally measured load and the measured effective crack length (see schematic in Fig. 6) were converted to the applied stress intensity factor using the stress intensity factor solution for compact tension specimens [15]. The crack length was measured for load levels corresponding to the P-CMOD curve in Fig. 4. The crack growth resistance versus crack length for the control specimens and for composites with a fiber volume fraction of 4 vol% is plotted in Fig. 5a and b, respectively. The symbols in the graphs represent the experimental data points for different test specimens. As is evident from Fig. 5b, the repeatability of the crack growth resistance curve is quite high. Logarithmic best-fit curve is drawn through the experimental data points (solid line) as the representative crack growth resistance curve. The K-curve, which satisfies $K = Ka$ and $\partial K/\partial a = \partial Ka/\partial a$ conditions, is also plotted. No apparent increase in crack growth resistance can be observed

for the control specimens. The critical stress intensity factor increased from 0.5 MPa $m^{1/2}$ for the control specimens to 2.5 MPa $m^{1/2}$ for the composites with 4 vol% of steel microfibers. The mechanisms that lead to the crack growth resistance behavior in composites reinforced with 4 vol% of microfibers are discussed in the following section.

3.3. Crack/aggregate and crack/fiber interactions during crack propagation

The *in-situ* crack propagation measurements are performed during loading using compact tension specimens. The crack in the control and fiber reinforced cementitious composites are monitored continuously and their crack path video taped. In Fig. 6 the cracking process is schematically illustrated for various load levels indicated on the P-CMOD curve. The crack extends from the precrack at point A and propagates in a stable manner (with increasing load) up to peak load. A discrete, but discontinuous crack is observed. The discontinuity in the crack path is associated with aggregate and fiber bridging sites in the crack wake as schematically illustrated in Fig. 6. Between load level B and C microcracks form at the aggregate/matrix interface at aggregate bridging sites in close vicinity to the notch tip. An aggregate bridging site at different load levels during the ascending branch of the P-CMOD is shown in Fig. 7a–d. The crack propagates from top to the bottom of the micrographs. The aggregate on the bottom of the micrographs is connected to both crack faces and constitutes a typical bridging site with frictional sliding occurring at the aggregate/matrix interface. Frictional sliding surfaces are indicated by arrows in Fig. 7a and b. During initial loading, the aggregate bridge may behave elastically. A load increase of 4%, opened the crack width between Fig. 7a and b except at the frictional sliding surfaces. At some load

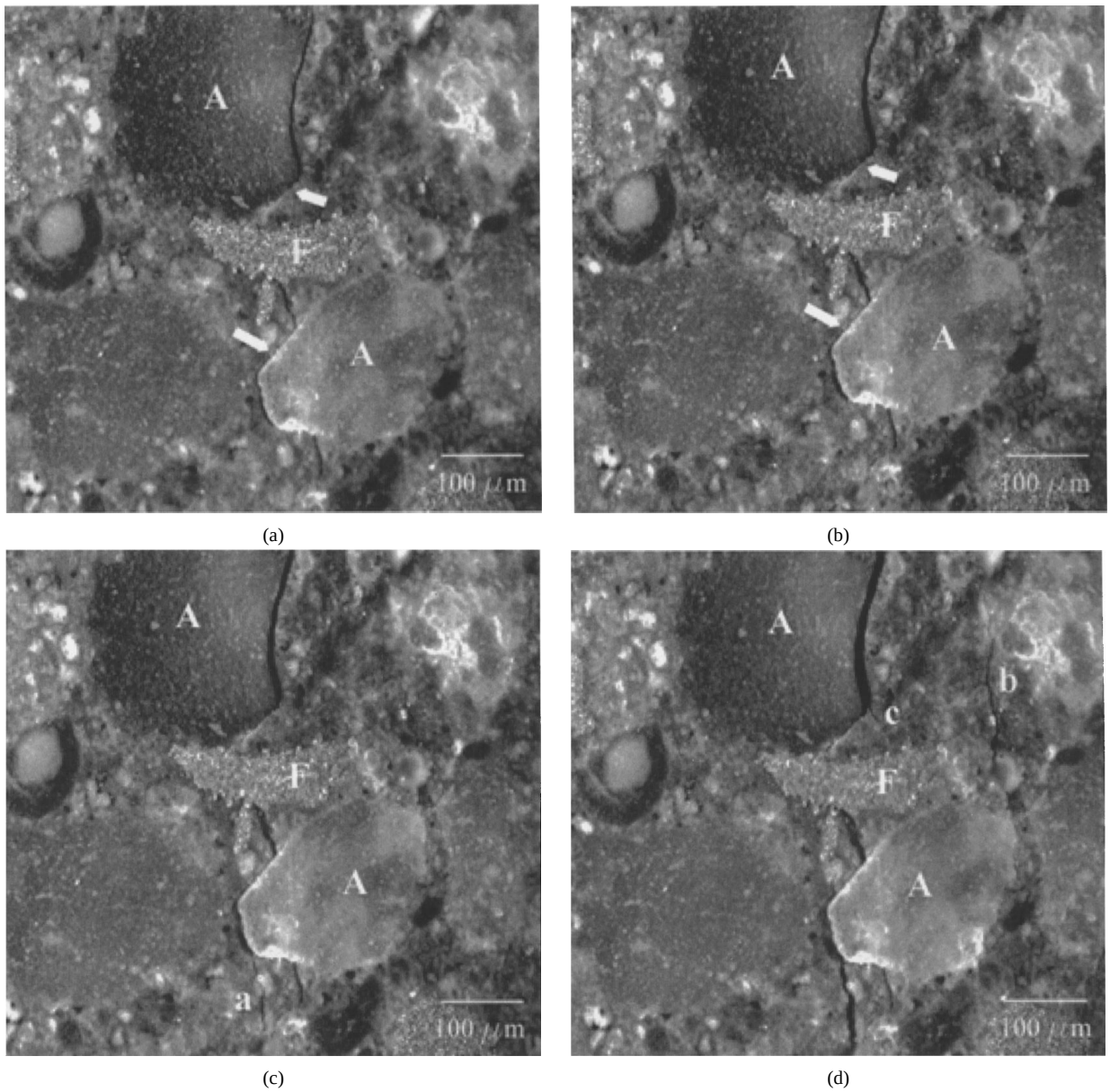

Figure 7 Aggregate bridging site in microfiber reinforced composites at different load levels during the ascending part of the P-CMOD curve. The load increase between a-b, b-c, and c-d are 4%, 7%, and 0.2%, respectively. A stands for aggregate, F for microfiber; arrows in a) point to frictional sliding surfaces along aggregate; secondary microcrack in c) is labeled “a” ; secondary microcracks observed in d) are labeled “b” and “c”.

level between b and c (load increase between b and c was 7%) the frictional traction along the mating surface at the bottom aggregate opened up a secondary crack (labeled a). A subsequent small load increase of 0.2% caused a new secondary crack to open up to the right of the aggregate (labeled b) and a smaller microcrack at the upper aggregate (labeled c) in Fig. 7d. Formation of secondary cracks at grain bridging sites due to frictional tractions are commonly observed in ceramic materials [16, 17]. When loads are sufficient to overcome the frictional resistance at the contact areas indicated by the arrows at the bridge/matrix interfaces aggregate pull-out occurs. The reduction in frictional resistance led to an increase in crack opening displacement of the main crack as observed in Fig. 7d. The frictional sliding resistance depends on the coefficient of friction of the interface and the normal stresses acting across the interface arising for example due to differential shrinkage or thermal expansion mismatch stresses. The work performed against these frictional bridging forces on crack opening has been shown to account for the majority of toughening observed in non-cubic monolithic ceramic materials [18]. While the aggregate on the bottom of the figure started to pull out of its socket during the applied load levels, no apparent changes have occurred at the fiber bridging site during these successive load applications.

Between load level C and D in Fig. 6, secondary cracks initiate at distances of 400–600 μm away from fiber bridging sites both in the crack wake and in the vicinity of the crack tip. A secondary crack that initiated to the right of the main crack adjacent to a fiber bridging site is shown in Fig. 8. The secondary crack extended in both directions (*i.e.* from both ends) and eventually joined the main crack ahead of the fiber bridging site at higher applied load levels. The energy absorption and hence toughness is considerably enhanced by the additional crack wake processes that are associated with these types of secondary crack formations. However, if the secondary crack forms in a region that is depleted of fibers (for example due to inhomogeneous fiber distribution), it propagates in an unstable fashion for quite some distance until it encounters fibers and incorporates them in its wake. The efficiency of the secondary cracks to contribute to strength and toughness enhancement depends strongly on the homogeneity of the fiber distribution. Emphasis has to be placed to ensure that the fibers are mixed homogeneously throughout the matrix.

Peak load D (Fig. 6) is accompanied by a distinct increase in the crack opening displacements along the crack profile. After the peak load, crack growth is considered unstable because the crack propagates initially under constant, then decreasing load. To observe bridging sites after the peak load, the load was slightly reduced which successfully arrested crack growth. Fiber bridging sites investigated beyond point E in the strain softening regime reveal secondary multiple microcrack formations along the fiber/matrix interface. Fig. 9a and b were taken at 90% of peak load and beyond peak load, respectively. The crack propagates from the top to the bottom of the micrograph, incorporating

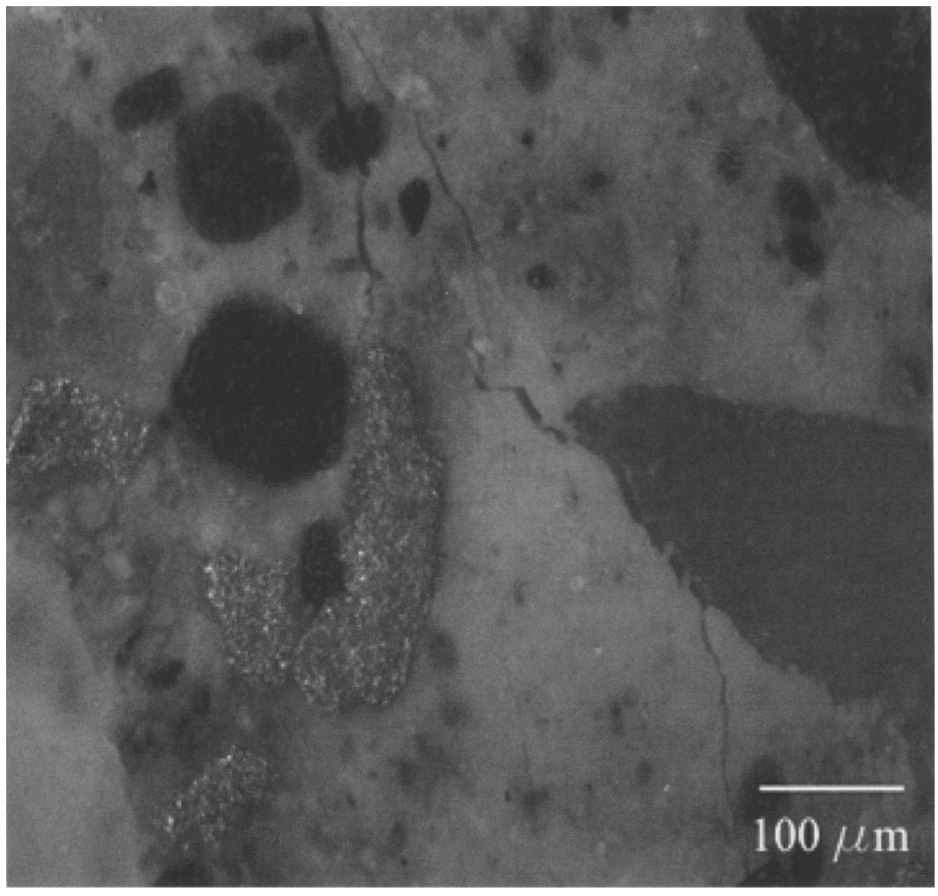

Figure 8 Secondary crack formation to the right of a fiber bridging site observed prior to peak load.

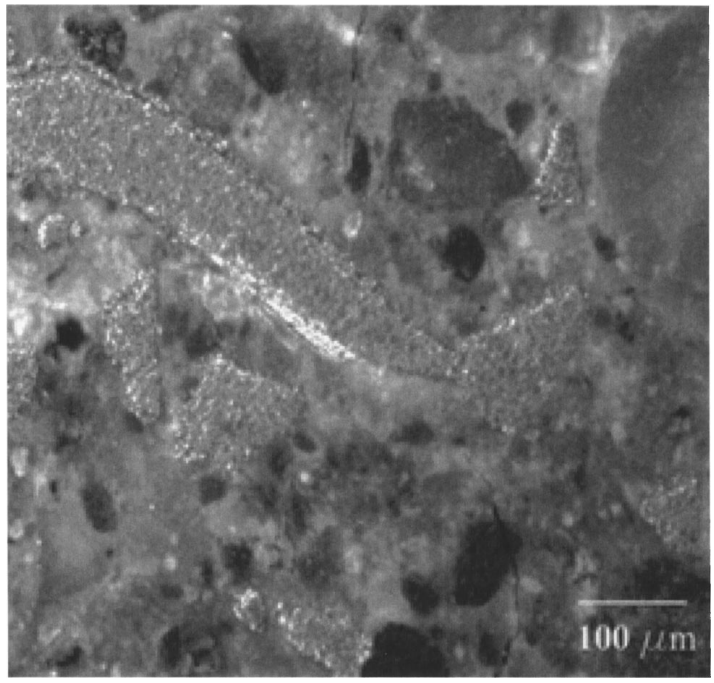

(a)

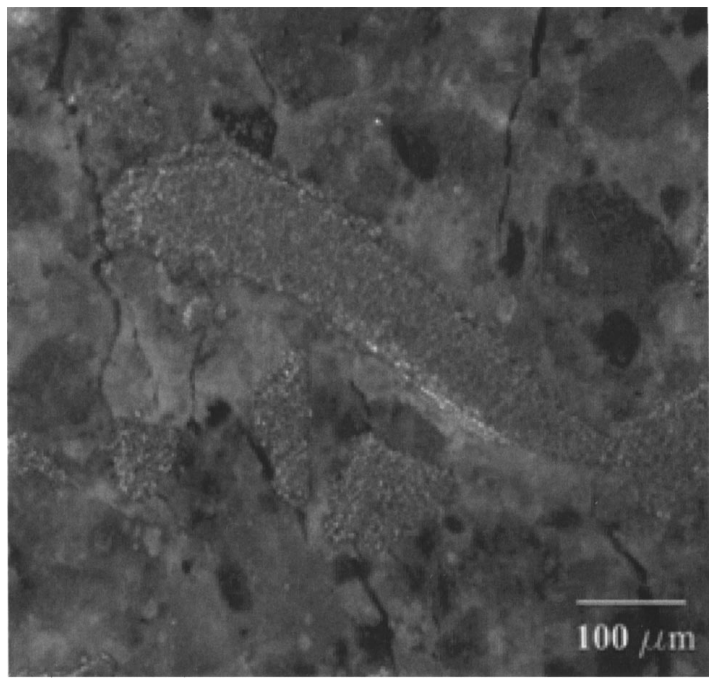

(b)

Figure 9 Fiber bridging site located close to the notch tip at 90% of peak load (a) and beyond peak load (b). The crack propagates from the top to the bottom of the micrograph. Secondary microcrack formations along the fiber/matrix interface away from the initial crack are seen in b).

the microfiber in its wake. The effectiveness of the microfiber in pinning the crack surfaces is revealed by the small crack opening displacement in the vicinity of the fiber (Fig. 9a). The small crack opening displacement is governed by the high interfacial frictional stress induced by the roughness of the fiber surface. Separation of the crack surfaces requires sliding along the fiber/matrix interface. The frictional sliding process may be responsible for the multiple secondary crack formations along the fiber/matrix interface (Fig. 9b). The first microcrack is commonly observed close to peak load on either side of the main crack. With increasing CMOD, more microcracks form successively along both sides of the fiber/matrix interface with increasing distance away from the main crack. Frequently, one of the microcracks coincides with the end of the fiber as seen in Fig. 9b and becomes the dominant crack. Consequently, fiber pullout, the dominant mechanism in conventional macrofiber reinforced composites is less frequently observed in these microfiber reinforced composites.

4. Summary

1) The splitting tension and the fracture tests reveal an increase in ultimate strength with increasing microfiber volume fraction.

2) The crack growth resistance behavior and the quasi-brittle behavior of steel microfiber reinforced composites is associated with crack wake toughening mechanisms.

3) Both aggregate and fiber bridging is taking place simultaneously during the strain hardening regime. Aggregate debonding and pullout was dominant during the ascending branch of the load-CMOD curve. Aggregate pullout was accompanied by the formation of secondary microcracks. The strain enhancement up to peak load may be reduced considerably in these microfiber composites if aggregate failure dominates over aggregate bridging and pullout.

4) Different types of secondary cracks in the vicinity of fiber bridging sites were observed at various load levels: I) During the ascending branch of the P-CMOD curve, secondary cracks initiate at a distance of 400–600 μm away from the fiber bridging site. II) At and beyond peak load, secondary microcracks formed along to the fiber/matrix interface. The secondary cracks are associated with high interfacial frictional shear stresses due to the roughness of the fiber surface. Fiber pullout, the dominant mechanism in conventional macrofiber reinforced composites was rarely observed.

5) The homogeneity in fiber distribution becomes very important in these composites. If the secondary cracks which initiate during the strain hardening regime in close vicinity of fiber bridging sites encounter fibers at onset and incorporate them as bridging sites in their wake, crack growth is retarded and additional cracks may open up in their vicinity. The more secondary cracks open up, the more energy will be absorbed at relatively small crack extensions. Considerable strength and toughness enhancement could then be obtained at even lower fiber volume fractions.

6) While these cracking processes and mechanisms lead to strength and toughness enhancement they may, however, deteriorate the fatigue properties.

Acknowledgments

This work was sponsored by the National Science Foundation under Grant No. CMS-962480.

References

1. H. H. HYNEN, Naval Civil Engineering Laboratory, Port Hueneme, Calif., Technical Report No. 979, 1, 1968.
2. S. MINDESS, L. CHEN and D. R. MORGAN, *Advn. Cem. Bas. Mat.* **1** (1994) 201.
3. N. BANTHIA, A. MONCEF, K. CHOKRI and J. SHENG, *Can. J. Civ. Eng.* **21** (1994) 999.
4. L. R. BETTERMAN, C. OUYANG and S. P. SHAH, *Adv. Cem. Bas. Mat.* **2** (1995) 53.
5. N. BANTHIA and J. SHENG, *Cement and Concrete Composites* **18** (1996) 251.
6. Y. SHAO, Z. LI and S. P. SHAH, *Advn. Cem. Bas. Mat.* **1** (1993) 55.
7. B. MOBASHER, H. STANG and S. P. SHAH, *Cem. Conc. Res.* **20** (1990) 665.
8. B. MOBASHER, A. CASTRO-MONTERO and S. P. SHAH, *Exp. Mech.* **30** (1990) 286.
9. J. AVESTON, G. COOPER and A. KELLY, in Conference Proceedings, National Phys. Laboratory, Guildford, UK, 1971 (IPC Science and Technology Press Ltd.) p. 15.
10. B. BUDIANSKY, J. W. HUTCHINSON and A. G. EVANS, *J. Mech. Phys. Solids* **34** (1986) 167.
11. D. MARSHALL, B. COX and A. G. EVANS, *Acta Metall.* **33** (1985) 2013.
12. L. M. MCCARTNEY, *Proc. Roy. Soc. London* **A 409** (1987) 329.
13. J. RODEL, J. F. KELLY, M. R. STOUDT and S. J. BENNISON, *Scanning Microscopy* **5** (1991) 29.
14. H. FREI and G. GRATHWOHL, *J. Phys. E: Sci. Instrum.* **22** (1989) 589.
15. H. TADA, P. C. PARIS and G. R. IRWIN, "The Stress Analysis Handbook" (Paris Production and Del Research Corp., St. Louis, MO., 1985).
16. J. RODEL, J. KELLY and B. J. LAWN, *Am. Cerm. Soc.* **73** (1990) 3313.
17. C. J. GILBERT, R. N. PETRANY, R. O. RITCHIE, R. H. DAUSKARDT and R. W. STEINBRECH, *J. Mater. Sci.* **30** (1995) 643.
18. G. VEKINIS, M. F. ASHBY and P. W. R. BEAUMONT, *Acta Metall. Mater.* **38** (1990) 1151.

Received 13 May 1999
and accepted 9 August 2000